Electronic Supplementary Material (ESI) for Environmental Science: Nano.


# Supporting Information

# Enhanced removal of As(III) by manganese doped defective UiO-66 coupled peroxymonosulfate: Multiple reactive oxygen species and system stability

# Characterization

The Zr-MOFs were characterized by Zeiss sigma500 scanning electron microscope (SEM) with an operating voltage of 10.0 kV, WD = 4.4 mm. The structure and composition of the Zr-MOFs were investigated by transmission electron microscope (TEM, FEI talos f200s 200 kV). The crystal phases of the Zr-MOFs were analyzed by X-ray diffractometer (XRD, D8 ADVANCE, Bruker, German). The X-ray photoelectron spectroscopy (XPS, Thermo ESCALAB 250Xi) and Fourier transform infrared spectroscopy (FTIR, Thermo Fisher Scientific, Nicolet iS 5) were employed to analyze the surface chemical properties of the Zr-MOFs before and after adsorption. The Brunauer-Emmett-Teller specific surface areas ($S_{BET}$) and pore size distribution of the materials were analysed by Micromeritics 2460 analyser (degassing temperature: 423.15k, degassing time:12 h). The zero charge point of the adsorbent, $pH_{pzc}$, was obtained from a zeta potential meter (Malvern Zetasizer Nano *ZS90*). Electron spin resonance (ESR) test for radicals detection was performed by Bruker A300. The total arsenic concentration was determined by inductively coupled plasma mass spectrometry (ICP-MS, Agilent, 7900, USA) and inductively coupled plasma atomic emission spectroscopy (ICP-OES, AViO 500 PerkinElmer).

# Analytical methods

The adsorption kinetics of arsenic were determined by fitting the data to a model based on pseudo-first order (Eq. (S1)) and pseudo-second order (Eq. (S2)); adsorptive capacity was calculated by:

$$q_e = (C_0 - C_e) \times \frac{V}{W}$$

where $q_e$ (mg $g^{-1}$) is equilibrium adsorption capacity of arsenic on $Mn_1D_{40}$UiO-66, $V$ (L) presents the volume of arsenic solution used in the experiment, $W$ (g) is the weight of the used $Mn_1D_{40}$UiO-66.

$$q_t = q_e\left(1 - e^{-k_1 t}\right) \quad \text{(S1)}$$

$$q_t = q_e\left(1 - \frac{1}{1 + q_e k_2 t}\right) \quad \text{(S2)}$$

where $q_e$ (mg $g^{-1}$) and $q_t$ (mg $g^{-1}$) are the adsorption capacity at equilibrium and at time $t$ (min), respectively, $k_1$ ($min^{-1}$) is the pseudo-first-order adsorption rate constant, $k_2$ (g $(mg \cdot min)^{-1}$) is the pseudo-second-order adsorption rate constant.

Langmuir (Eq. (S3)) and Freundlich (Eq. (S4)) isotherm models were utilized to fit the adsorption isotherms based on Eq. (S3) and Eq. (S4):

$$q_e = \frac{q_{max} K_L C_e}{1 + K_L C_e} \quad \text{(S3)}$$

$$q_e = K_F C_e^{\frac{1}{n}} \quad \text{(S4)}$$

where $C_e$ (mg $L^{-1}$) is the equilibrated arsenic concentration within the solvent phase, $q_e$ (mg $g^{-1}$) is the amount of arsenic adsorbed by $Mn_1D_{40}$UiO-66, $q_{max}$ (mg $g^{-1}$) is the maximum adsorption capacity, $K_L$ is the Langmuir constant of adsorption, $K_F$ and $n$, respectively, are the Freundlich model constants.

# Tables

**Table S1** $S_{BET}$ and pore volume parameters of $Mn_1D_{40}UiO$-66.

| Samples | $S_{BET}$ ($m^2$ $g^{-1}$) | Vp ($cm^3$ $g^{-1}$) |
|---|---|---|
| UiO-66-0 | 952.92 | 0.58 |
| $D_{40}UiO$-66 | 1306.09 | 0.71 |
| $Mn_1D_{40}UiO$-66 | 1273.13 | 0.68 |

**Table S2** Langmuir and Freundlich constants for arsenic adsorption by $Mn_1D_{40}UiO$-66.

| Items | T℃ | Langmuir model | | | Freundlich model | | |
|---|---|---|---|---|---|---|---|
| | | $q_{max}$ (mg $g^{-1}$) | $K_L$ (L $mg^{-1}$) | $R^2$ | $K_F$ (mg $g^{-1}$) | n | $R^2$ |
| As(III) / $Mn_1D_{40}UiO$-66 / PMS | 25℃ | 112.47429 | 0.60005 | 0.92597 | 41.60568 | 2.63259 | 0.98191 |
| As(III) ) / $Mn_1D_{40}UiO$-66 | 25℃ | 14.5589 | 0.55433 | 0.90227 | 5.99905 | 3.44643 | 0.99464 |

**Table S3** $k_{obs}$ with different pH, different concentrations of anions and different concentrations of humic acid.

| Variable condition | Reaction condition | $k_{obs}$ ($min^{-1}$) |
|---|---|---|
| pH | pH = 3 | 0.0527 |
| | pH = 5 | 0.0546 |
| | pH = 7 | 0.0563 |
| | pH = 9 | 0.0695 |
| | pH = 11 | 0.140 |
| Anions | 5 mM $SO_4^{2-}$ | 0.0178 |
| | 10 mM $SO_4^{2-}$ | 0.0174 |
| | 5 mM $Cl^-$ | 0.0240 |
| | 10 mM $Cl^-$ | 0.0221 |
| | 5 mM $NO_3^-$ | 0.0365 |
| | 10 mM $NO_3^-$ | 0.0357 |
| | 5 mM $CO_3^{2-}$ | 0.0033 |
| | 10 mM $CO_3^{2-}$ | 0.0035 |
| HA | HA = 0 mg $L^{-1}$ | 0.0752 |
| | HA = 25 mg $L^{-1}$ | 0.0635 |
| | HA = 50 mg $L^{-1}$ | 0.0483 |
| | HA = 100 mg $L^{-1}$ | 0.0491 |

**Table S4** Results of shell-by-shell fitting from EXAFS data.

| Sample | Atomic path | [a]CN | [b]R(Å) | [c]$\sigma^2$(Å) | [e]R-factor |
|---|---|---|---|---|---|
| $Mn_1D_{40}$UiO-66-As | As-O | 4 | 1.79 | 0.001 | 0.016 |
| | As-Zr | 1.5 | 3.50 | 0.013 | |

[a]CN: coordination number; $\sigma^2$: Debye-Waller factor; [b]R: interatomic distance; [e]R-factor: goodness of fitting

**Table S5** Characteristics of the natural water samples.

| Items | Value |
|---|---|
| TOC (mg $L^{-1}$) | 2.07 |
| TC (mg $L^{-1}$) | 2.07 |
| pH | 3.22 |
| Cd (mg $L^{-1}$) | 0.151 |
| Mn (mg $L^{-1}$) | 10.846 |
| Fe ((mg $L^{-1}$) | 0.141 |
| Co (mg $L^{-1}$) | 0.050 |
| Ni (mg $L^{-1}$) | 0.068 |
| Cu (mg $L^{-1}$) | 0.116 |
| Zn (mg $L^{-1}$) | 42.000 |
| $SO_4^{2-}$ (mg $L^{-1}$) | 1472.84 |
| $Cl^-$ (mg $L^{-1}$) | 7.6905 |
| $NO_3^-$ (mg $L^{-1}$) | — |
| $CO_3^{2-}$ (mg $L^{-1}$) | 17.135 |

# Figures

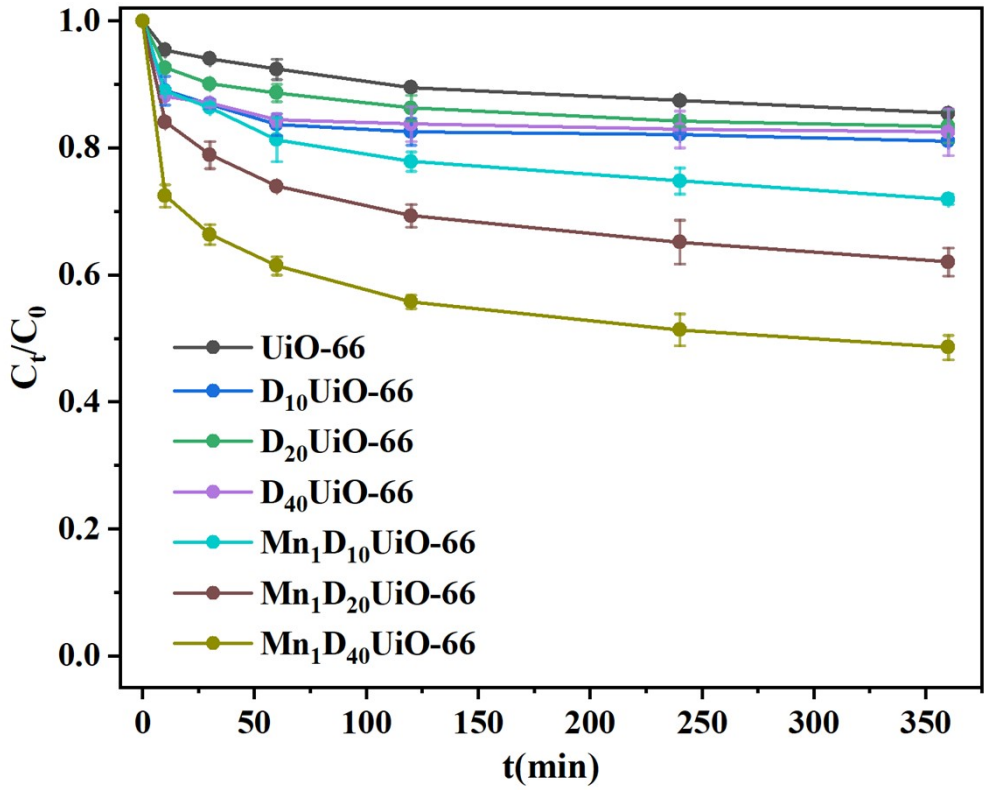


**Fig. S1.** As(III) removal efficiency by $Mn_xD_nUiO$-66, $C_{catalyst}$ = 0.2 g $L^{-1}$, $C_{0(As)}$ = 1 mg $L^{-1}$.

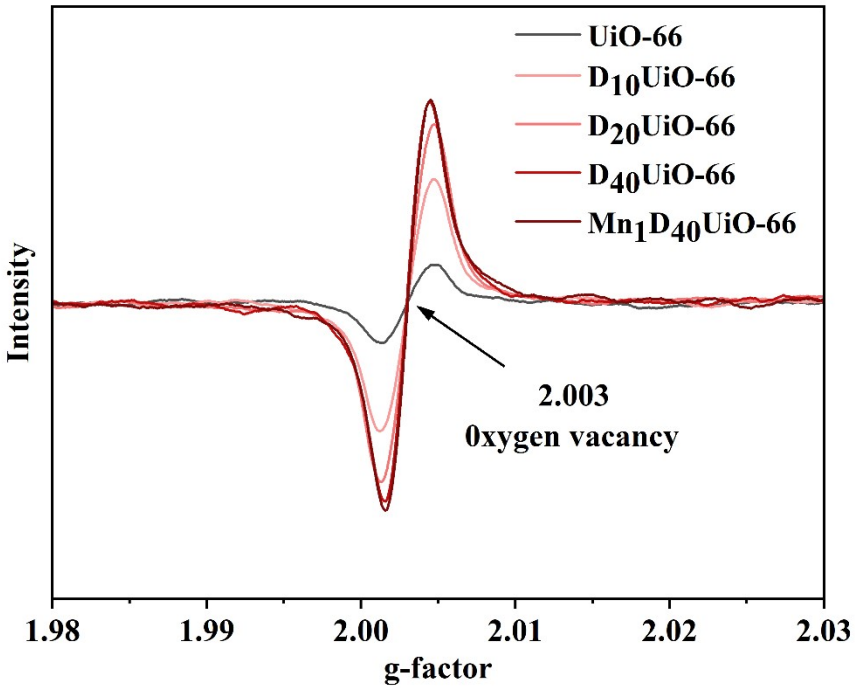


**Fig. S2.** ESR spectra of $D_n$UiO-66 samples and $Mn_1D_{40}$UiO-66.

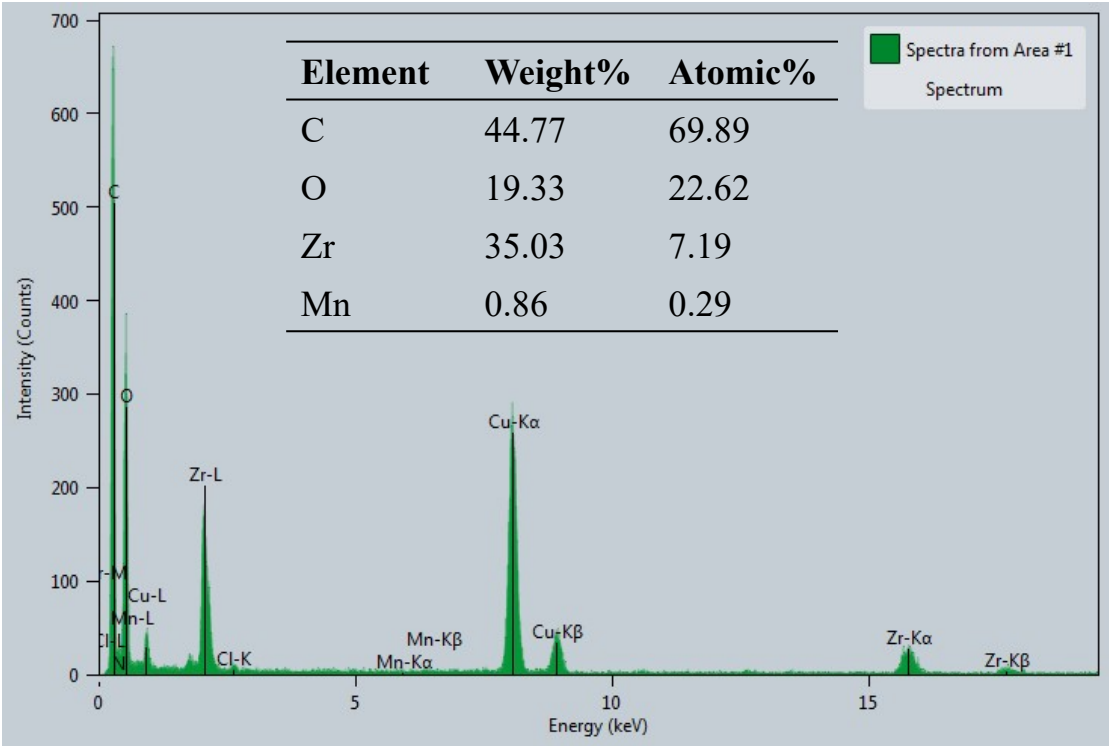


**Fig. S3.** EDS spectrum of $Mn_1D_{40}$UiO-66.

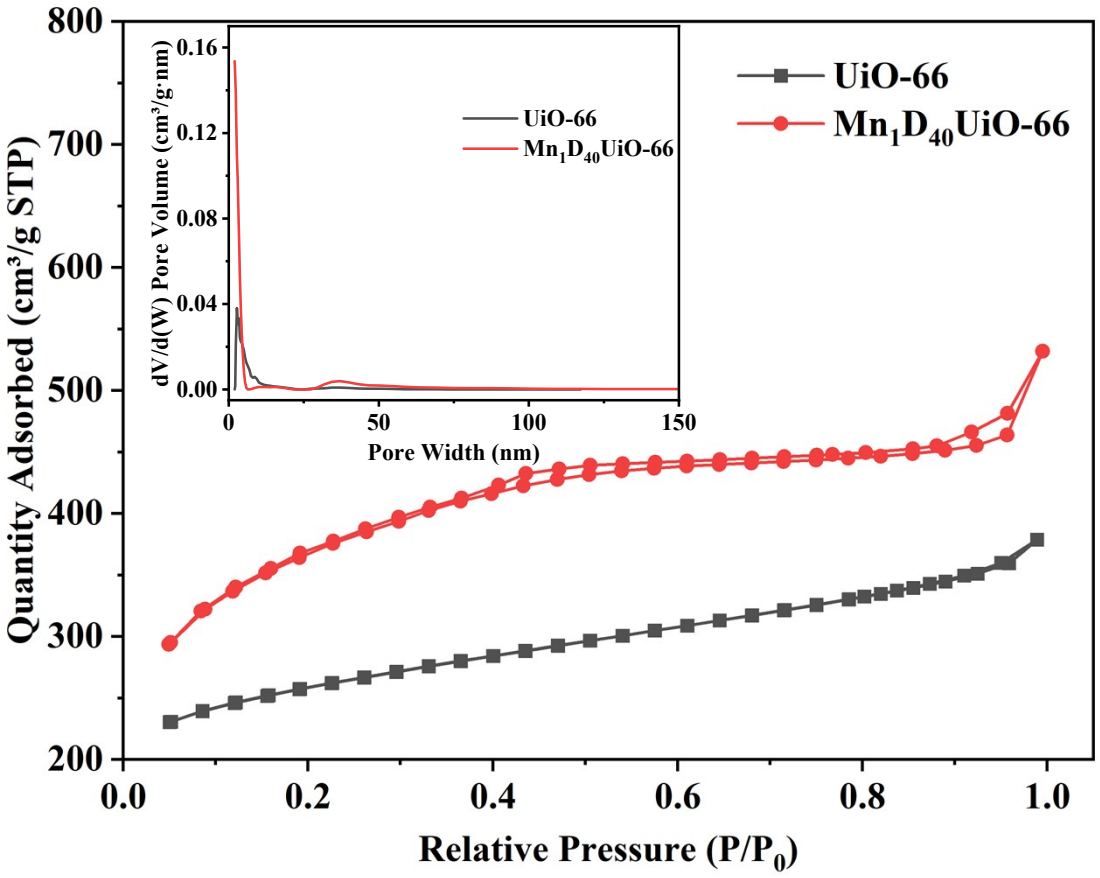


**Fig. S4.** The $N_2$ adsorption-desorption isotherms of $Mn_1D_{40}$UiO-66.

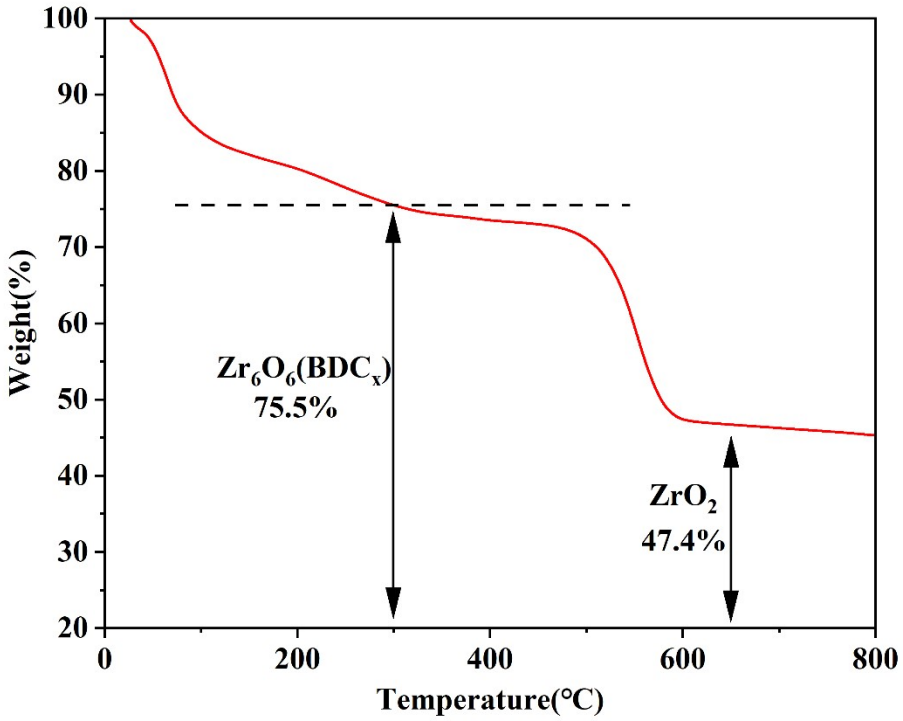


**Fig.S5.** TGA analysis of $Mn_1D_{40}$UiO-66.

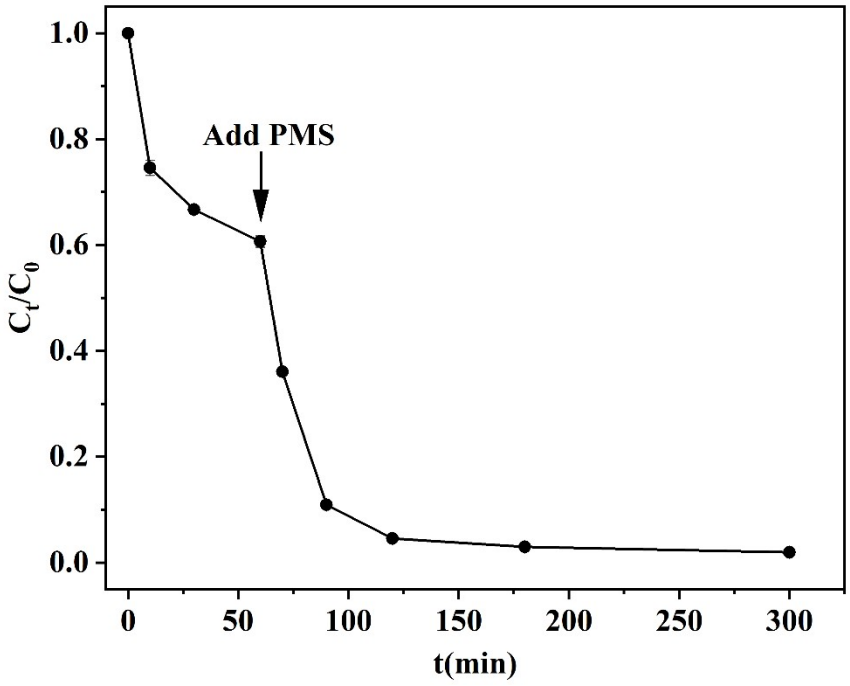


**Fig. S6.** Effect of adding PMS midway, $Mn_1D_{40}UiO\text{-}66$ = 0.2 g $L^{-1}$.

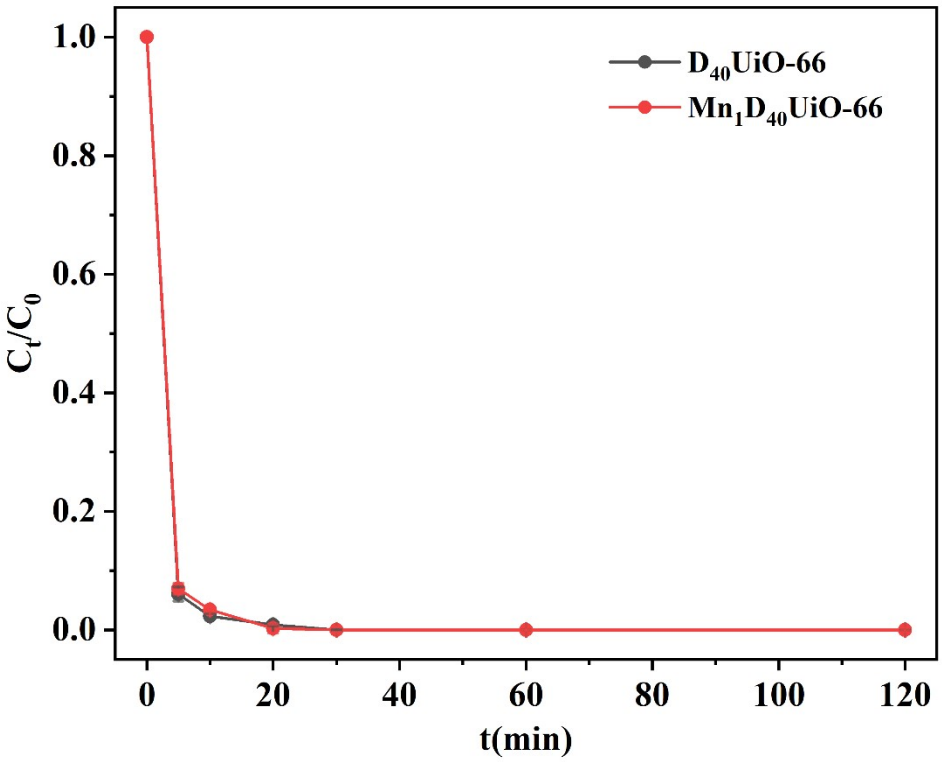


**Fig. S7.** Adsorption kinetics of As(V) by $Mn_1D_{40}UiO-66$ and $D_{40}UiO-66$, $C_{catalyst}$ = 0.2 g $L^{-1}$, $C_{0(As)}$ = 1.1 mg $L^{-1}$.

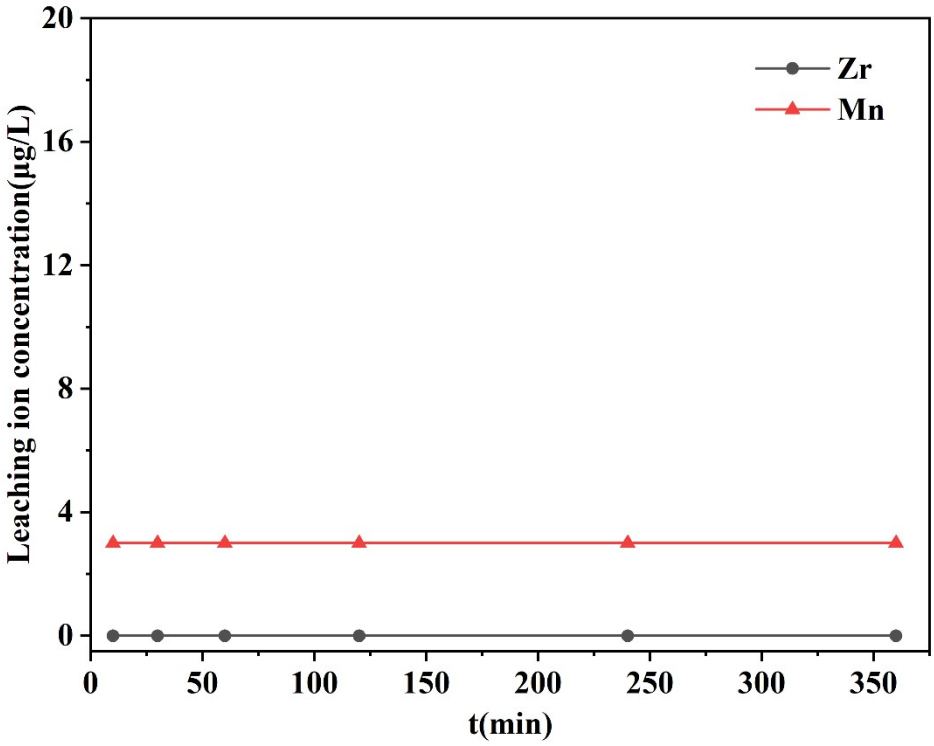


**Fig. S8.** Leaching of Zr and Mn during reactions in $Mn_1D_{40}$UiO-66 / PMS system.

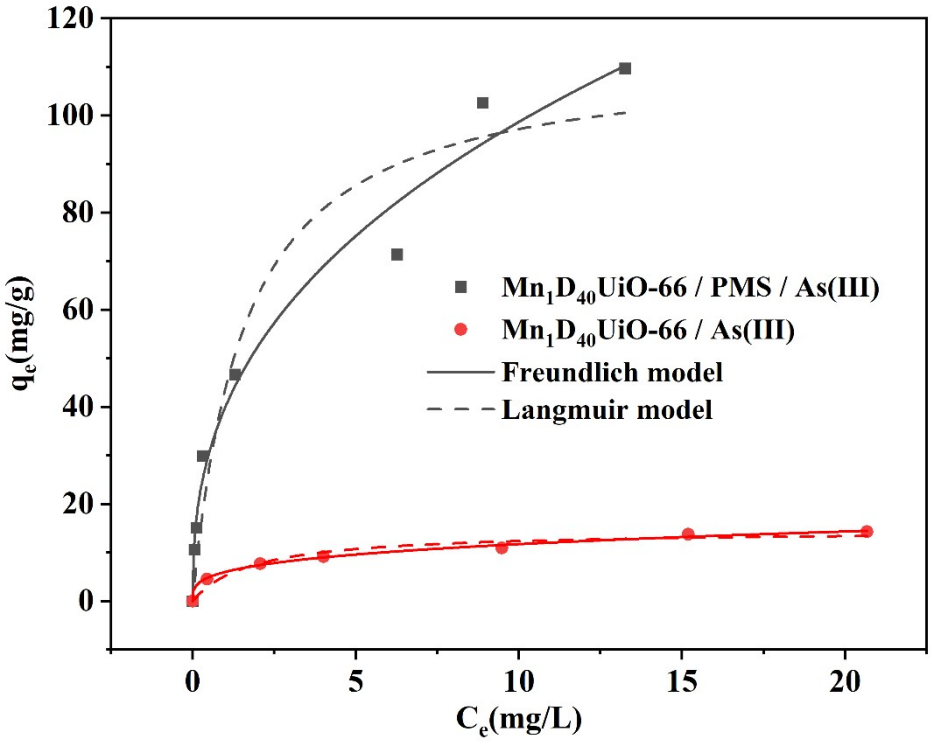


**Fig. S9**. Adsorption isotherms of As(III) by $Mn_1D_{40}$UiO-66 with or without PMS.

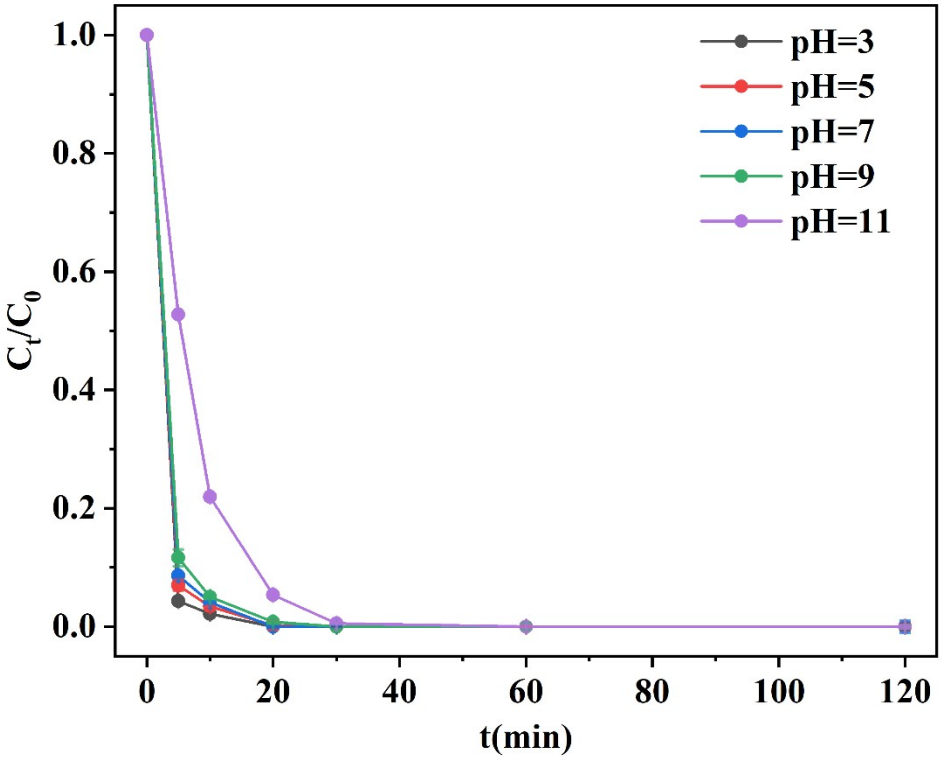


**Fig. S10.** Adsorption kinetics of As(V) by $Mn_1D_{40}$UiO-66. $Mn_1D_{40}$UiO-66 = 0.2 g $L^{-1}$, $C_{0(As)}$ = 1.1 mg $L^{-1}$.

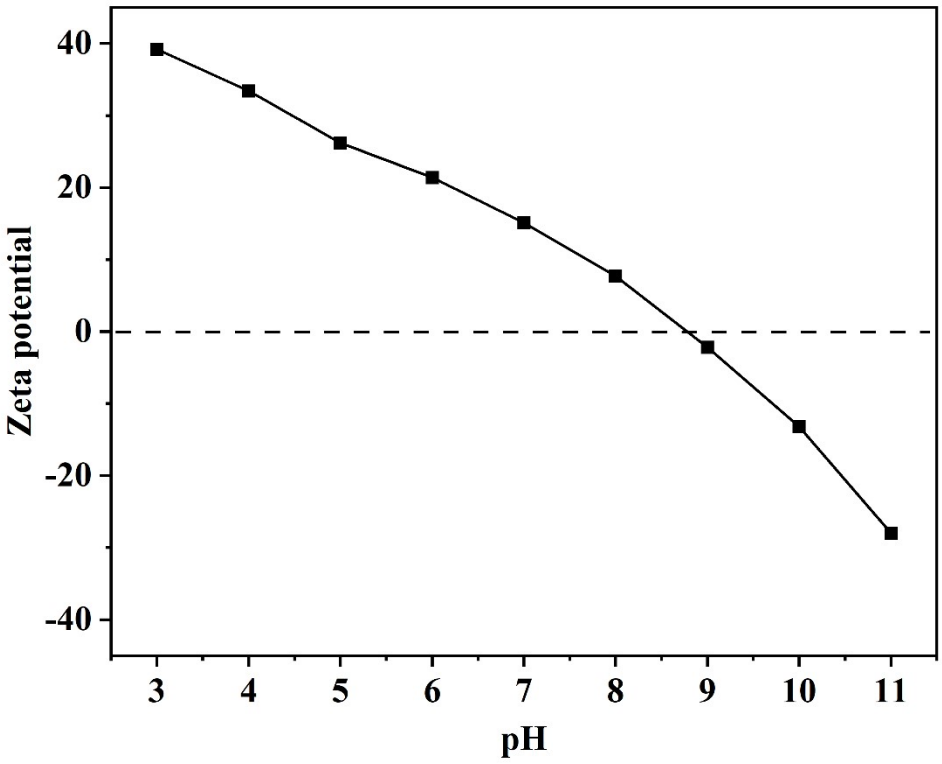


**Fig. S11**. Zeta potentials of $Mn_1D_{40}$UiO-66.

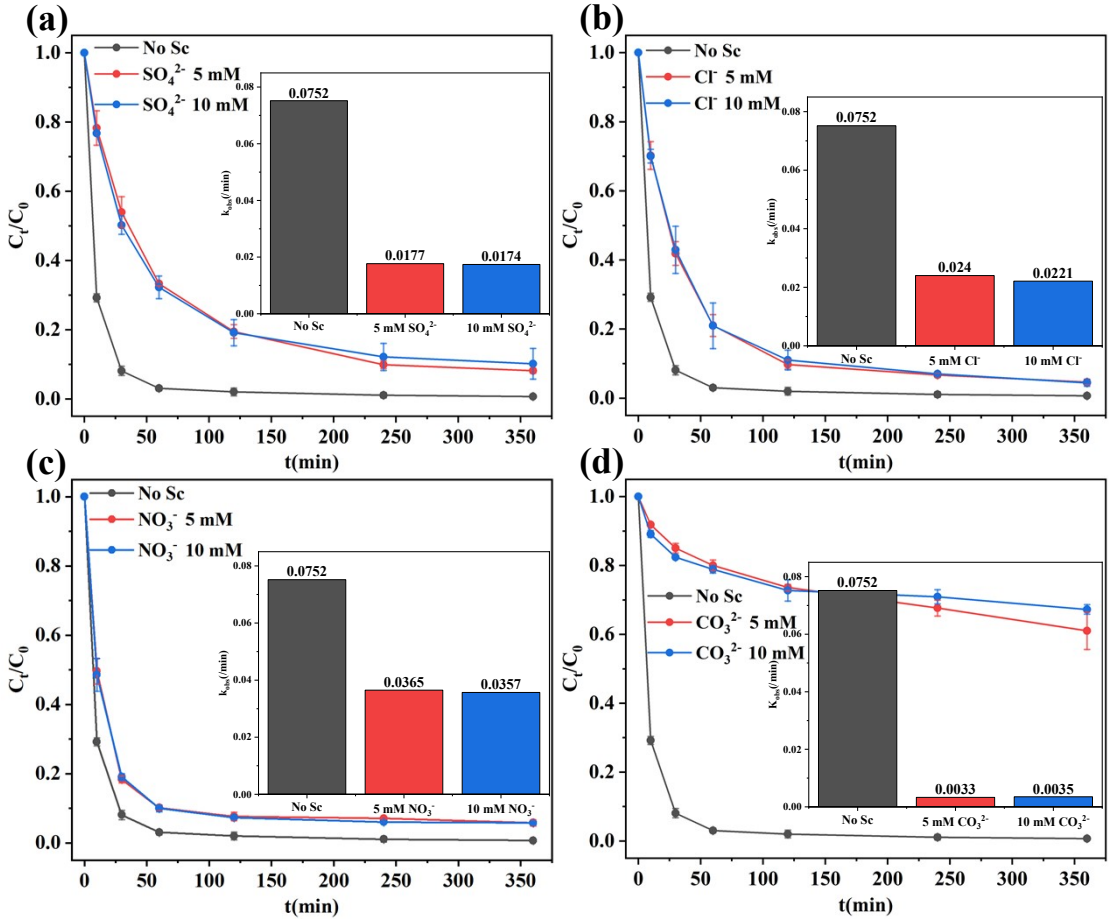


**Fig. S12.** The effect of solution anions on As(III) removal, $Mn_1D_{40}$UiO-66 = 0.2 g $L^{-1}$, $C_{PMS}$ = 0.1 mM, $C_{0(As)}$ = 1.1 mg $L^{-1}$.

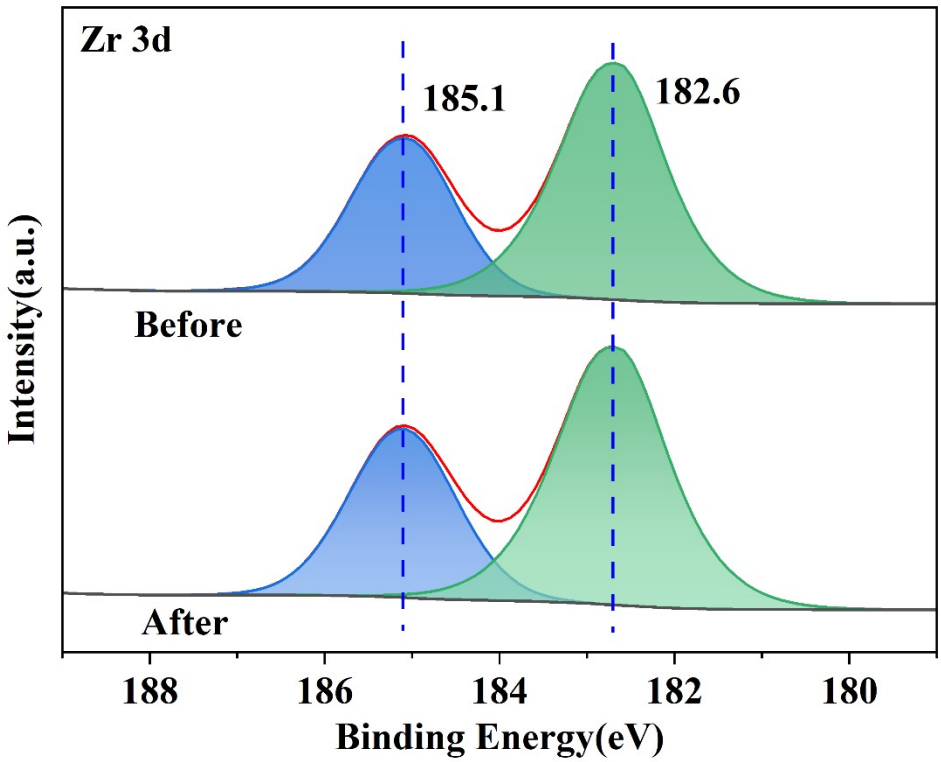


**Fig. S13.** Zr 3d XPS spectra.

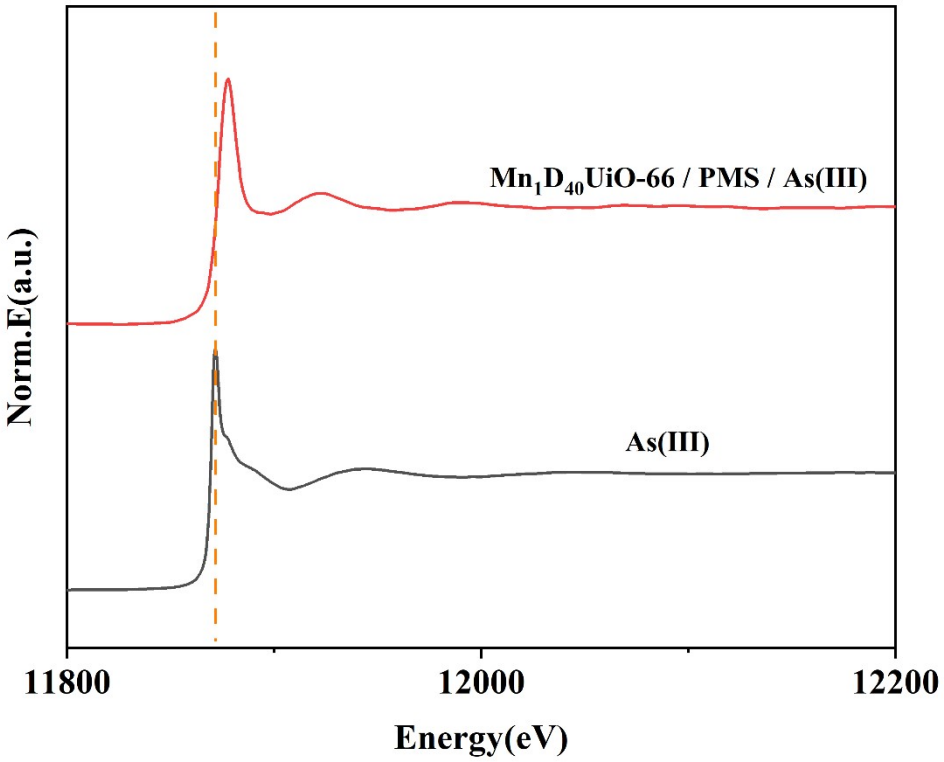


**Fig. S14** Normalized As K-edge EXAFS spectra of $As_2O_3$ and $Mn_1D_{40}$UiO-66 after adsorption.

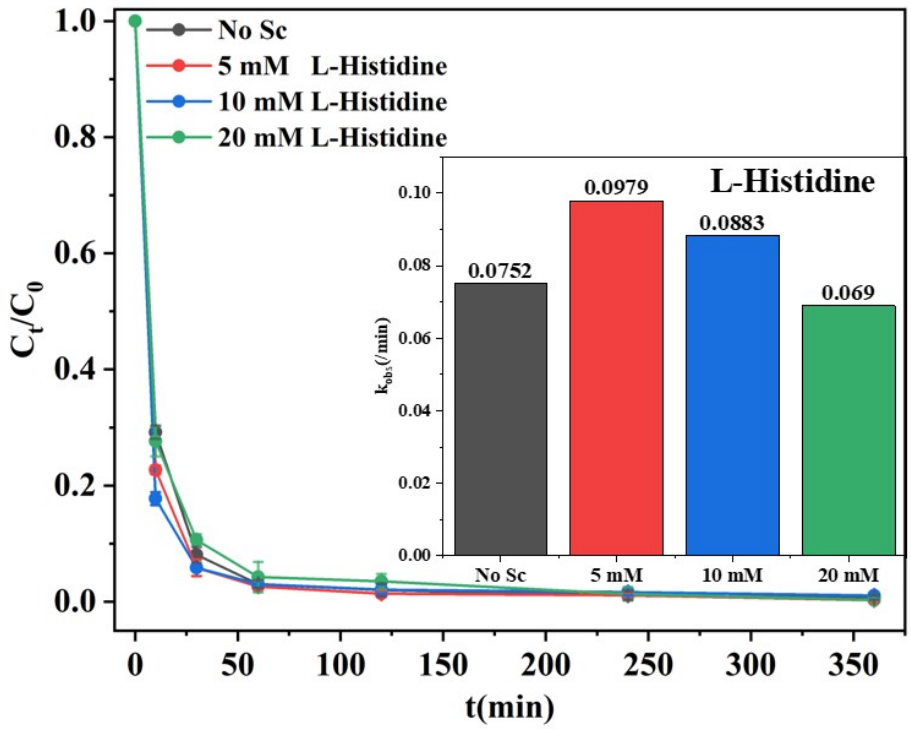


**Fig. S15.** Adsorption kinetics of As(III) with L-Histidine, $Mn_1D_{40}UiO$-66 = 0.2 g $L^{-1}$, $C_{PMS}$ = 0.1 mM, $C_{0(As)}$ = 1.1 mg $L^{-1}$.

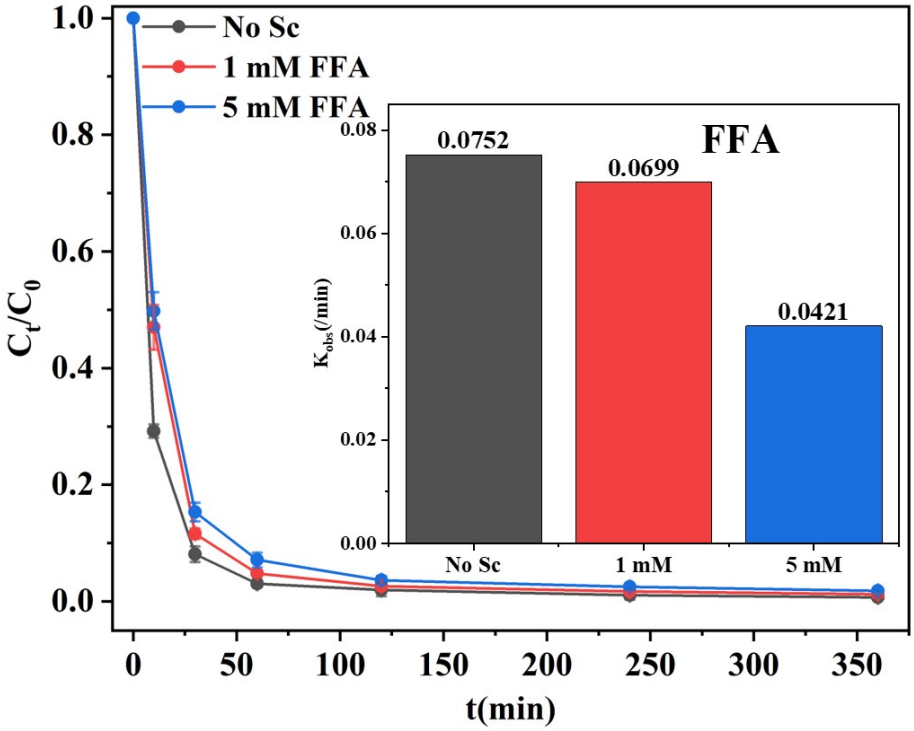


**Fig. S16.** Adsorption kinetics of As(III) with FFA, $Mn_1D_{40}$UiO-66 = 0.2 g $L^{-1}$, $C_{PMS}$ = 0.1 mM, $C_{0(As)}$ = 1.1 mg $L^{-1}$.

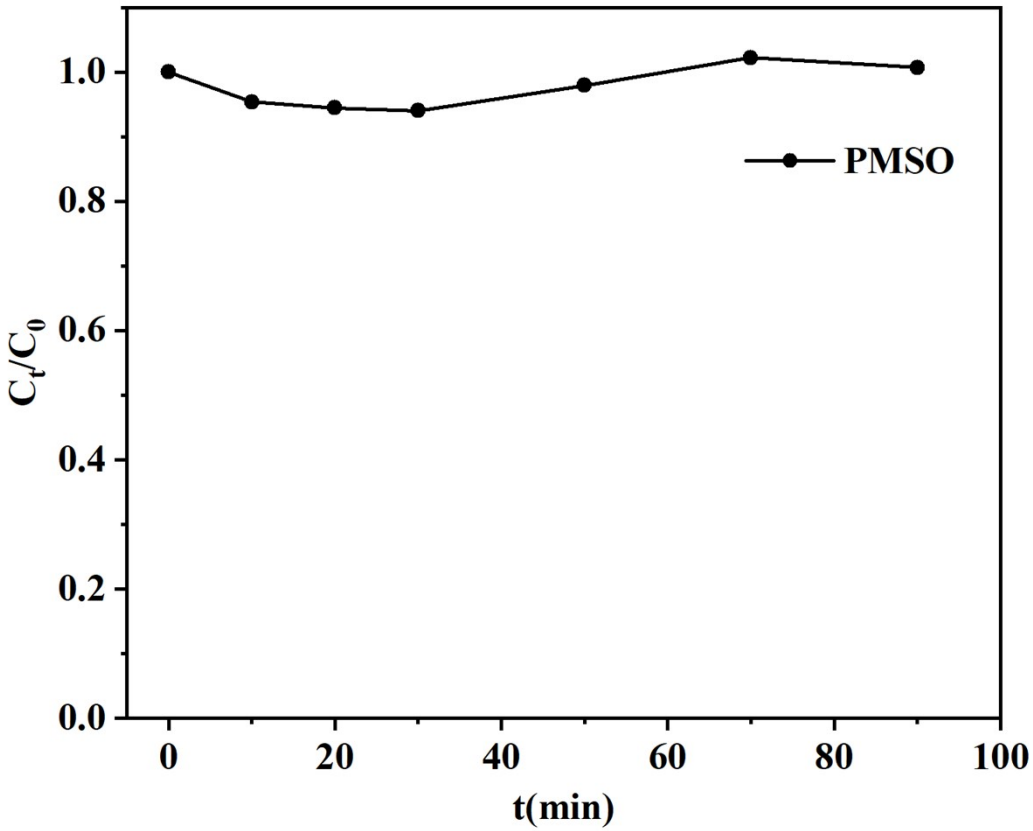


**Fig. S17.** Variation in the concentration of PMSO. $C_{PMSO}$ = 10 μM.

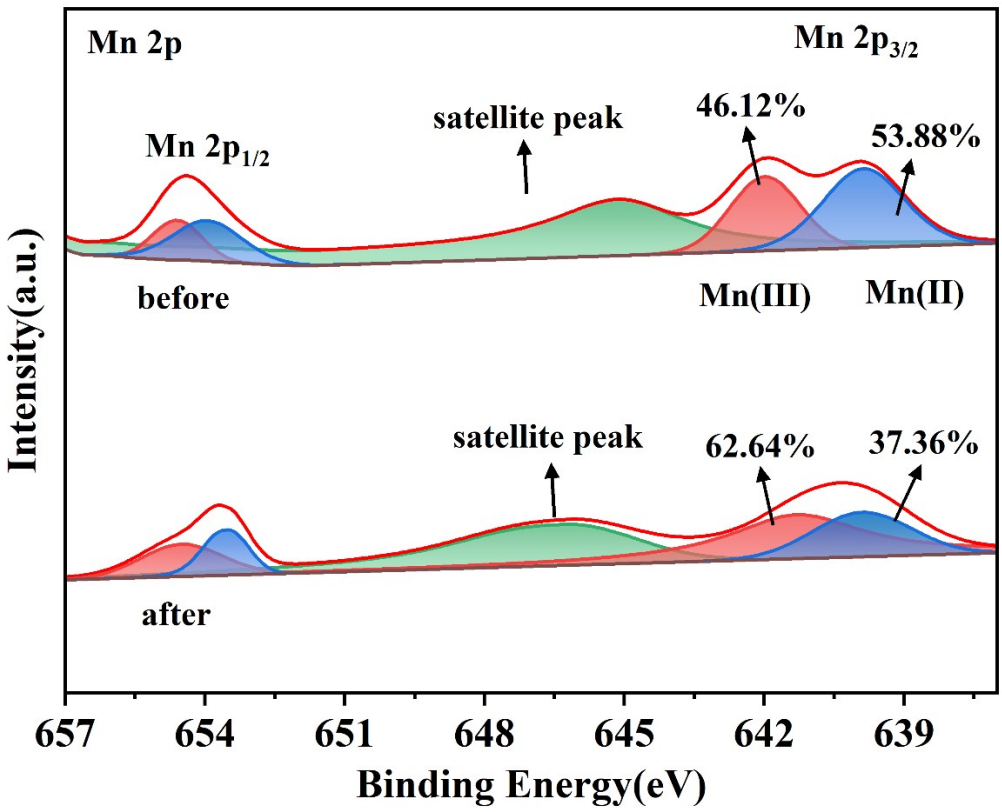


**Fig. S18.** Mn 2p XPS spectra.

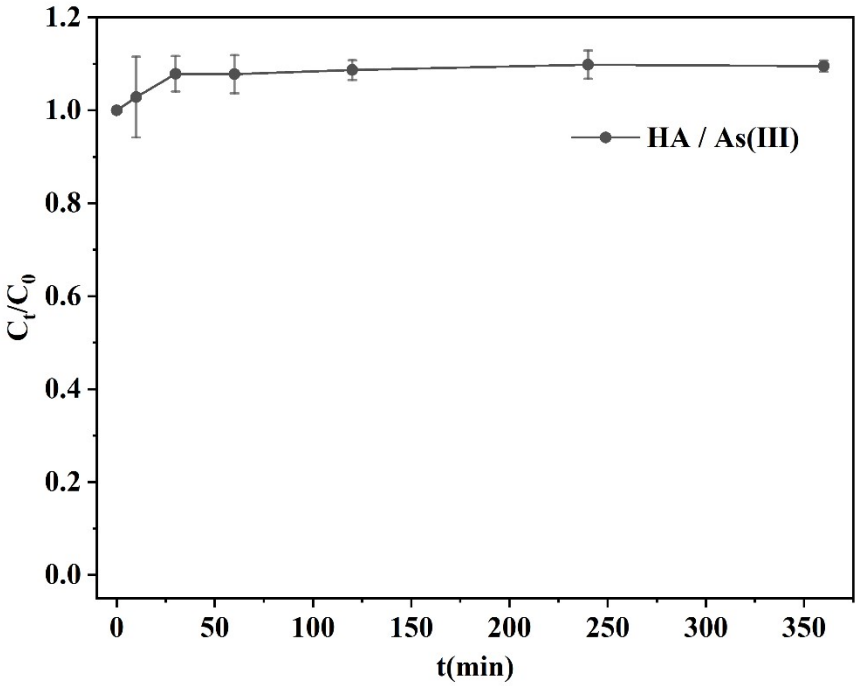


**Fig. S19.** As(III) concentration in the HA / As(III) system, $C_{HA}$ = 100 mg $L^{-1}$.

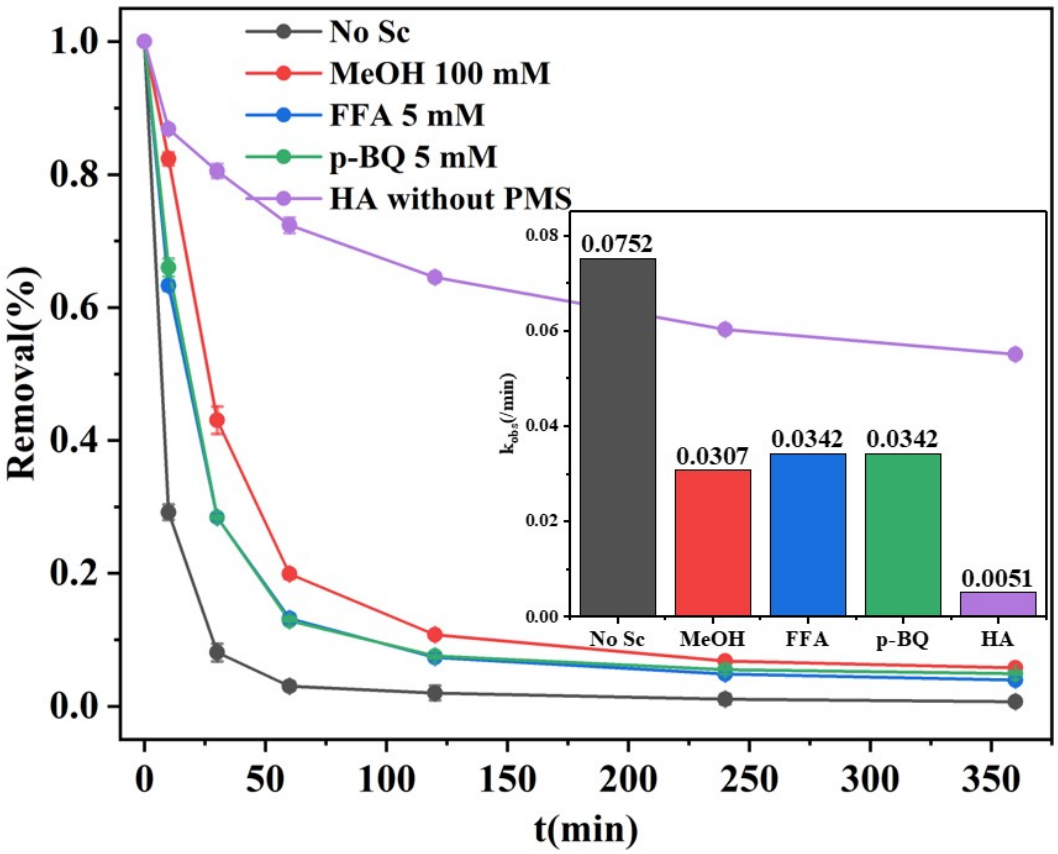


**Fig. S20.** Adsorption kinetics of As(III) by HA / $Mn_1D_{40}$UiO-66 / PMS with different scavengers, $Mn_1D_{40}$UiO-66 = 0.2 g $L^{-1}$, $C_{PMS}$ = 0.1 mM, $C_{0(As)}$ = 1.1 mg $L^{-1}$.

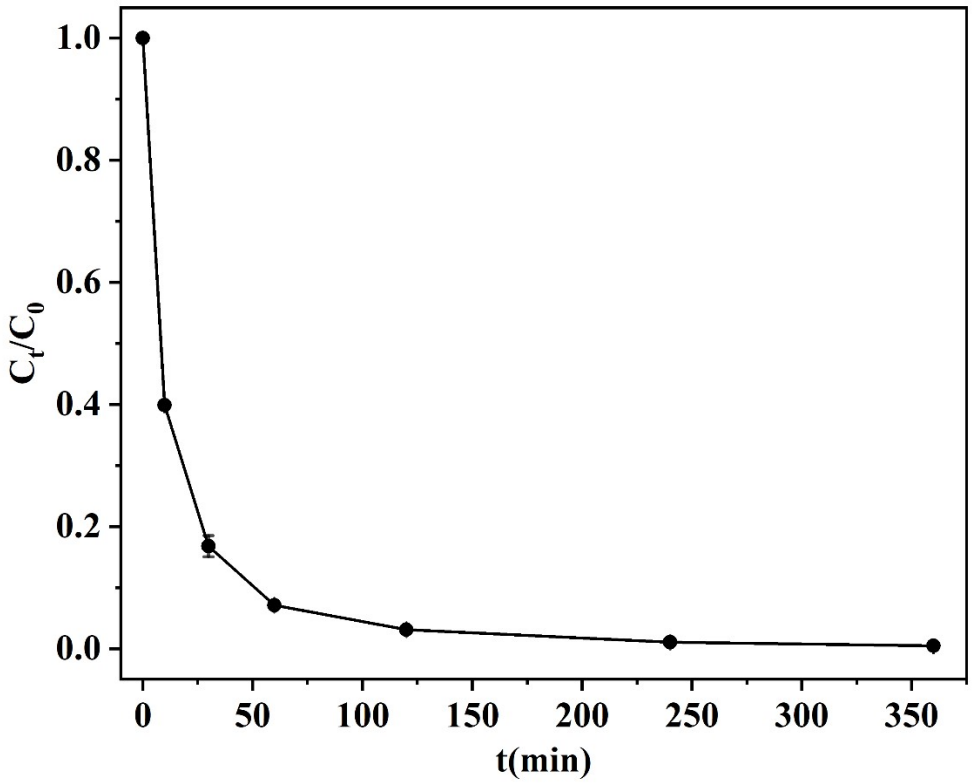


**Fig. S21.** As(III) removal in natural water samples, $Mn_1D_{40}$UiO-66 = 0.2 g $L^{-1}$, $C_{PMS}$ = 0.1 mM.

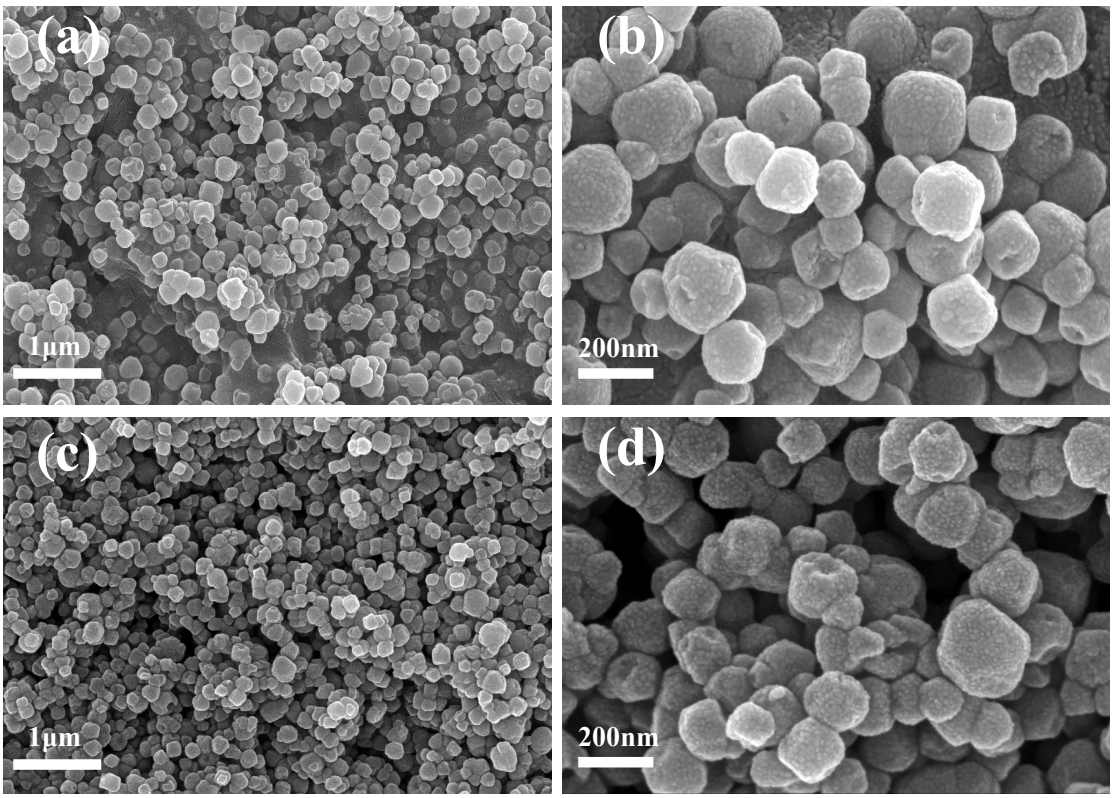


**Fig. S22.** SEM images of $Mn_1D_{40}$UiO-66 before and after adsorption.

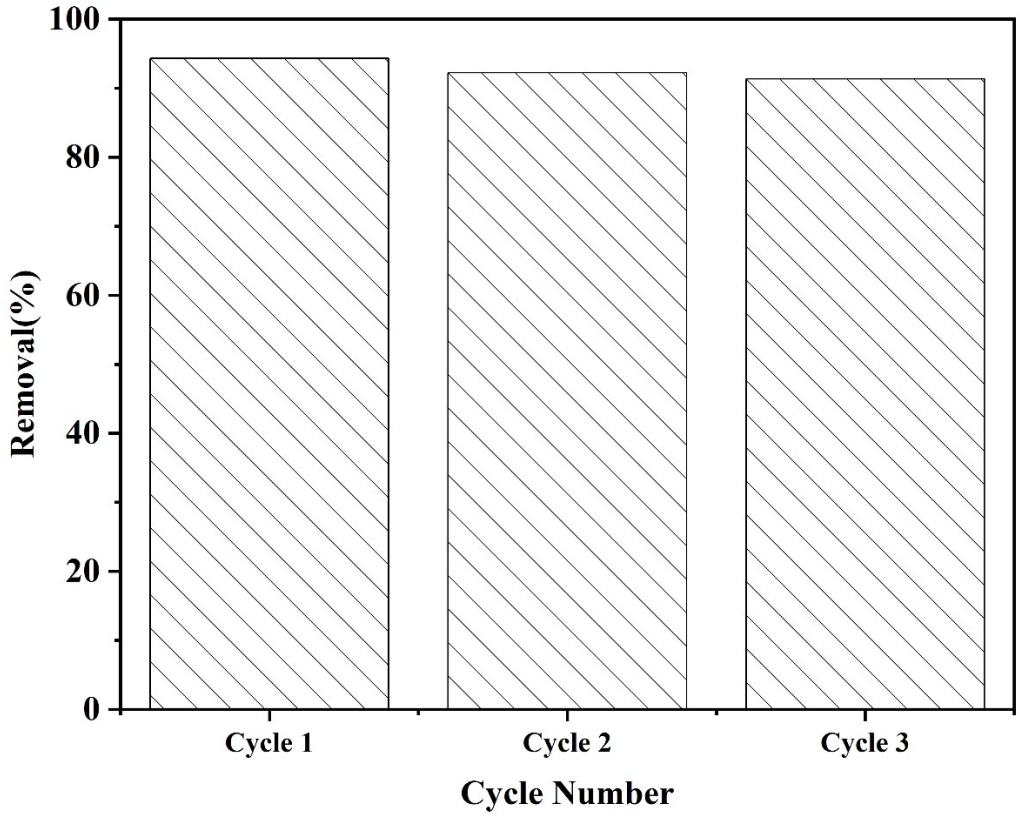


**Fig. S23.** Recycling of $Mn_1D_{40}UiO$-66 / PMS for As(III) removal, $Mn_1D_{40}UiO$-66 = 0.2 g $L^{-1}$, $C_{PMS}$ = 0.1 mM, $C_{0(As)}$ = 1 mg $L^{-1}$.